

In vivo MRS assessment of altered fatty acyl unsaturation in liver tumor formation of a TGF α /c-myc transgenic mouse model

J. Griffiths,^{*,†} Y. Tesiram,^{*} G. E. Reid,^{§,**} D. Saunders,^{*} R. A. Floyd,^{††} and R. A. Towner^{1,*,†}

Advanced Magnetic Resonance Center,^{*} and Experimental Therapeutics,^{††} Oklahoma Medical Research Foundation, Oklahoma City, OK 73104; Pathology Department,[†] University of Oklahoma Health Sciences Center, Oklahoma City, OK 73104; and Department of Chemistry,[§] and Department of Biochemistry and Molecular Biology,^{**} Michigan State University, East Lansing, MI 48824

Abstract Current detection methods (computed tomography, ultrasound, and MRI) for hepatocarcinogenesis in humans rely on visual confirmation of neoplastic formations. A more effective early detection method is needed. Using in vivo magnetic resonance spectroscopy (MRS), we show that alterations in the integral ratios of the bis-allyl to vinyl hydrogen protons in unsaturated lipid fatty acyl groups correlate with the development of neoplastic formations in vivo in a TGF α /c-myc mouse hepatocellular carcinoma (HCC) model. HPLC analysis of the TGF α /c-myc mice liver tissue revealed a significant increase in the amount of oleic acid, along with alterations in linoleic and γ -linolenic acids, as compared with control CD1 mice. Electrospray ionization tandem mass spectrometry analysis indicated a significant increase in the abundance of specific glycerol phosphatidylcholine (GPCho) lipids containing palmitic and oleic acids between control CD1 and TGF α /c-myc mice liver tissue extracts. Western blot analysis of the mice liver tissue indicates alterations in the desaturase enzyme stearoyl CoA desaturase (SCD)1, responsible for palmitic and oleic acid formation. Microarray analysis detected alterations in several genes involved with fatty acid metabolism, particularly SCD2, in transgenic mouse liver tissue. In correlation with the HPLC, mass spectrometry, Western blot, and microarray analyses, we are able to confirm the ability of in vivo MRS to detect precancerous lesions in the mouse liver before visual neoplastic formations were detectable by MRI.—Griffiths, J., Y. Tesiram, G. E. Reid, D. Saunders, R. A. Floyd, and R. A. Towner. In vivo MRS assessment of altered fatty acyl unsaturation in liver tumor formation of a TGF α /c-myc transgenic mouse model. *J. Lipid Res.* 2009. 50: 611–622.

Supplementary key words unsaturated fatty acids • tumor lipid metabolism • liver cancer • magnetic resonance spectroscopy • mice

Support for the studies was provided by funding from the Oklahoma Medical Research, the Oklahoma Center for the Advancement of Sciences and Technology (OCAST), grant of fMRI-2, Molecular Image Inc. (Menlo Park, CA), and National Institutes of Health grant RO1CA82506.

Manuscript received 20 May 2008 and in revised form 21 July 2008 and in re-revised form 14 November 2008 and in re-re-revised form 5 December 2008.

Published, JLR Papers in Press, December 8, 2008.
DOI 10.1194/jlr.M800265-JLR200

Hepatocellular carcinoma (HCC) is one of the most deadly forms of cancer in the world. The World Health Organization reports that liver cancer is the third highest cause of death from cancer, with HCC being predominantly observed in Asian and African countries (1). There are many known causes of HCC, including hepatitis B and C, cirrhosis, and aflatoxin exposure. The techniques currently used for diagnosis of liver cancer rely on imaging modalities (MRI, computed tomography, and ultrasound) that, at the highest sensitivity, are able to detect evidence of neoplasia when there is a formation of at least 1 mm. Image confirmation of a neoplasm this size usually only occurs at a later stage in cancer development when therapy treatments are not as effective. Therefore, the prognosis for a patient when they have visual evidence of neoplasia is poor. Additionally, neoplasms at the lower range of imaging detection are often unverifiable without biopsy. There is a need, therefore, to develop a method that can detect neoplastic formations at an earlier stage than those now in use.

The efficacy of utilizing MRI, which mainly detects only protons from water hydrogens, for hepatic tumor detection and the measurement of tumor volumetric growth has been established previously (2, 3). We have utilized MRI in this study for visual confirmation of neoplastic tissue formations in the TGF α /c-myc mouse liver tumor model. In addition to the MRI visible liver changes, there have been several metabolic alterations in lipid processes and composition noted in association with HCC. Alterations in cholesterol have been shown to occur, with decreases in cholesterol coinciding with patient mortality

Abbreviations: CSI, chemical shift imaging; DU, degree of unsaturation; FDR, false discovery rate; FADS1, fatty acid desaturase 1; FADS2, fatty acid desaturase 2; GPCho, glycerol phosphatidylcholine; GPE, glycerol phosphatidylethanolamine; HCC, hepatocellular carcinoma; MRS, magnetic resonance spectroscopy; PC, phosphatidylcholine; PE, phosphatidylethanolamine; PI, precursor ion; ROI, region of interest; SCD, stearoyl CoA desaturase; TE, echo time; TR, relaxation time.

¹To whom correspondence should be addressed.

e-mail: rheal-towner@omrf.org

(4). It has been reported that glycerol phosphatidylethanolamine (GPE) increases in concentration in hepatocyte nodules resulting in a decreased glycerol phosphatidylcholine (GPCho)/GPE ratio (4).

The main components of phospholipids, fatty acids, are known to have effects in cellular signaling. Fatty acids are involved in apoptosis and cell-cycle regulation (4, 5). Fatty acid synthesis along the ω -6 pathway results in the production of prostaglandins and leukotrienes that are an integral part of the apoptotic pathway (4, 6). Certain desaturase enzymes involved in fatty acid synthesis such as stearoyl-CoA desaturase (SCD) and fatty acid desaturase 2 (FADS2 or Δ 6 desaturase), are known to contribute to high oleic and low γ -linolenic acid levels, respectively, in hepatoma cells (4, 7). Abel et al. (4) found that the levels of MUFA were increased in rat hepatocyte nodules over time. The PUFA γ -linolenic has been noted to have anticancer effects in cells with an increase in lipid peroxidation leading to apoptosis of the cells (6, 8). The observation of metabolic alterations in the fatty acid profile of the liver in vivo would seem to be a valid technique to utilize for hepatocarcinogenic nodules and tumors.

Magnetic resonance spectroscopy (MRS), which can be used to assess hydrogen-containing molecules other than water as observed by MRI, has been used in numerous studies to identify alterations in metabolites associated with various cancers (9–12). MRS has also been used to quantify levels of total choline compounds in the human breast as a diagnosis tool for suspicious lesions (9). It has been previously established using single-voxel MRS, that changes in the lipid profiles of tumor tissue during the stages of development are observable with proton MRS (13). Alterations in the methyl and methylene hydrogens from lipid resonances were noted using MRS (13). The Foley et al. (13) study also showed that there were increases in the unsaturated methylene hydrogens found in PUFA at 2.8 ppm and increases in the unsaturated lipid olefinic hydrogens at 5.4 ppm during hepatocarcinogenesis. Previous research in our lab has shown the ability of two-dimensional spectroscopy to characterize PUFA species from the resonances at 2.8 and 5.3 ppm (14). In this study, we wanted to determine the efficacy of utilizing MRS to measure the degree of unsaturation (DU) of the bis-allyl and vinyl lipid hydrogens at 2.8 and 5.3 ppm, respectively, in association with nodule and tumor development in a TGF α / *c-myc* transgenic HCC model in vivo. Our work has shown that by taking a ratio of the integral values of the peaks of the lipid hydrogens at 2.8 ppm and 5.3 ppm, we can determine the DU of the fatty acids in tissue lipids. Ex vivo smooth muscle research by Singer et al. (11) also utilized the ratio of methylene protons between sites of unsaturated protons for determining the DU. He et al. (10) also looked at the lipid signals resonating at 2.8 and 5.3 ppm in a human breast cancer study.

Chemical shift imaging (CSI) is a MRS technique where multiple voxels in a grid pattern acquire metabolic information across a wide area inside a tissue of interest. Each of the voxels in a CSI scan produces a separate and unique spectrum apart from its neighbor. Essentially, CSI detects

in vivo the tissue distributions of metabolites (10). CSI has been utilized to monitor biochemical and metabolic phenotypic changes noninvasively in animals and humans (10, 15–17). CSI has also been utilized to detect intracranial mobile lipids in the rat brain utilizing an ultrashort echo time (TE) (18). Another study showed promise in the use of CSI as a noninvasive method of differentiating malignant skeletal tumors from nonmalignant tissue (19).

In this study, we wanted to determine the efficacy of utilizing MRS CSI to measure the DU of the bis-allyl and vinyl lipid hydrogens at 2.8 and 5.3 ppm, respectively, in association with nodule and tumor development in a TGF α / *c-myc* transgenic HCC model in vivo. We have found that an alteration in this DU value correlates with liver neoplasia in a transgenic mouse model of hepatocarcinogenesis.

METHODS

Animal model

A transgenic mouse model of hepatocarcinogenesis was used as the experimental model in this study ($n = 20$). These transgenic mice have mutations in the transcriptional regulator *c-myc* as well as the cell growth factor TGF α (20, 21). The transgenic mice develop a primary form of liver cancer that has many similar features to that observed in humans (20, 21). CD1 mice were used as the nontransgenic controls in this study ($n = 6$). All mice were routinely monitored for any signs of discomfort or severe illness. Animal weights were taken at each of the MRI/MRS analysis time points; there was no correlation between the changes in the animal's body weight and the onset of neoplastic formations. Mice were euthanized using CO₂ gas asphyxiation. Liver tissue was immediately removed from the mice upon euthanasia. Liver tissue sections were removed from the tumorous regions in the transgenic mice at the time of sacrifice of the animals and sent for histologic preparation. H and E stains of the liver tissue were performed. The experiments were carried out in conformity with NIH policy and with the Oklahoma Medical Research Foundation's Institutional Animal Care and Use Committee approval.

MRI and MRS

All of the MRI and MRS data were collected on a Bruker Biospec 7.0 Tesla/ 300MHz small animal 30 cm horizontal bore spectrometer USR 70130(Oklahoma City, OK). The analysis time points for this study were 20, 26, 30, 34, and 40 weeks of age for the control and transgenic mice. There were five transgenic mice scanned at 40 weeks of age; 15 transgenic mice were scanned at 34 weeks; 20 transgenic mice were scanned at 20, 26, and 30 weeks. Each transgenic mouse was scanned more than once in the MRI and MRS study, up to its time of sacrifice in the time point study. The same six control mice were scanned at each time point of the study and then sacrificed at the last time point of 40 weeks. At least five transgenic mice were sacrificed at each time point for in vitro analysis and additional control mice were purchased for in vitro tissue analysis at all time points. A multiring bird-cage coil was utilized in this study. A gradient echo fast low angle shot scan was utilized to obtain the 12 multislice images of the mice, with a TE of 5.35 ms, a relaxation time (TR) of 189.12ms, a flip angle of 60°, eight averages, a 256 \times 256 matrix, spatial resolution of 150 μ m, and a total acquisition time of 8 min. The field of view on all scans was 38.4 mm \times 38.4 mm with a slice thickness and slice gap both of 1 mm. ¹H-MRS data were obtained, utilizing MRI images for anatomical positioning, with a CSI scan. Parameters

for the CSI scan were: a TE of 3.5 ms, a TR of 1,500 ms, water suppression, a 38.4 mm × 38.4 mm field of view, and an acquisition time of 30 min. A total of 1,024 scans were taken and averaged together for each MRS scan. A matrix of 32 × 32 voxels, or regions of interest (ROIs), were used to obtain multiple spectra from all areas of a single centrally located 1.5 mm thick slice in the liver. During MRI/MRS analysis, the animals were anesthetized using 2–3% Isoflurane and 100% oxygen respiration was constantly monitored using a respiration pillow and SAM PC gating software (SAI Instruments, Manchester, England). To process the data, the software program Mathematica was utilized. Magnitude spectra processed by Paravision software was imported into Mathematica. A ratio of the bis-allyl to vinyl hydrogen protons near unsaturated bonds in fatty acids was taken to produce the DU measurement (12). Using Mathematica, we were able to correlate the MRS data of DU values with a corresponding MRI anatomical image. Lesions that were visually apparent on MRI images at 34 and 40 weeks of age were correlated with CSI data sets of spectra. ROIs were selected at earlier time points (20, 26, and 30 weeks) in the CSI data sets corresponding to regions of MRI apparent lesions at 34 and 40 weeks. The curve in Fig. 3 was generated utilizing pure standards and was based off of previously published work in our lab (12).

HPLC

The lipids were extracted from liver tissue of the transgenic and control mice at various time points, following a modified Folch extraction method where a 2:1 chloroform to methanol mixture with 0.01% butylated hydroxytoluene was used to extract the lipids after tissue homogenization, and a sodium sulfate filled funnel was used to remove excess water (22). The various lipid classes in the liver sample were separated by thin layer chromatography (TLC) utilizing a mobile phase of 50:25:8:4 chloroform/methanol/glacial acetic acid/water v/v. Individual GPCho and GPE lipids were removed from the TLC plates, saponified, and the subsequent separated fatty acids were then esterified to produce fatty acid phenacyl-esters (23). The phenacyl-ester extracts were analyzed for alterations in the fatty acid profile using a gradient HPLC method utilizing a 75:25 v/v HPLC grade acetonitrile to water ratio as mobile phase A, and 100% acetonitrile as mobile phase B. A reverse phase LC-18 250 × 4.6 mm column (Supelco) was used, and absorbance of the fatty acids was detected with a UV/Vis detector at 242 nm. Peak areas were measured for each fatty acid of interest in the chromatogram. Student's *t*-test of independent samples was performed for all analyses. Data values are displayed as mean ± SE. Solvents were all filtered HPLC grade, purchased from Honeywell Burdick and Jackson (Morristown, NJ). Pure standards for oleic, linoleic, γ -linolenic, and arachidonic acids were purchased from Sigma-Aldrich (St. Louis, MO). Pure standards were used to determine retention times of the individual fatty acids, and a standard curve of each pure fatty acid standard was obtained. These standards were chosen for this study due to their high levels in hepatocytes and for their possession of unsaturated bonds of importance to this study.

nESI-MS and MS/MS

Lipids were extracted from 200 mg liver tissue of the transgenic and control mice at 30 weeks, following a modified Folch extraction method where a 2:1 chloroform/methanol mixture was used to extract the lipids after tissue homogenization, and a sodium sulfate filled funnel was used to remove excess water (22). Lipid extracts were then dried under a stream of N₂ and stored at -70°C prior to analysis. Dried lipid extracts were resuspended in 500 μ l of methanol/chloroform (1:1 v/v), then aliquots were diluted 1:20 in isopropanol/methanol/chloroform (4:2:1 v/v)

containing 20 mM NH₄OH and 1.6 μ M 1,2-ditetradecanoyl-sn-glycero-3-phosphocholine (GPCho_(14:0/14:0)). Samples were then introduced to a Thermo Fisher model TSQ Quantum Ultra triple quadrupole mass spectrometer (San Jose, CA) via a chip-based nano-electrospray ionization (nESI) source (Advion NanoMate, Ithaca, NY) operating in infusion mode using an ESI HD chip A, a spray voltage of 1.4 kV, a gas pressure of 0.3 psi, and an air gap of 2 μ l. The ion transfer tube of the mass spectrometer was maintained at 150°C. All MS and MS/MS spectra were acquired automatically by methods created using the Xcalibur software (Thermo Fisher, San Jose, CA). In MS mode, the Q1 peak width was maintained at 0.5 Th. For precursor ion (PI) MS/MS scans, Q1 was operated at a peak width of 0.4 Th, while Q3 was maintained at 0.5 Th. For product ion scan mode MS/MS experiments, Q1 and Q3 were operated with peak widths of 1.0 Th. The Q2 collision gas pressure was set at 0.5 mtorr. MS and MS/MS scans were typically acquired using scan rates of 500 *m/z* second⁻¹. Collision energies were individually optimized for each lipid class-specific product ion or PI scan mode MS/MS experiment.

Identification of GPCho lipids was initially achieved using a lipid class specific PI scan mode experiment to monitor for the characteristic phosphocholine product ion at *m/z* 184 (PI 184). Then, assignment of the acyl substituents present in each of the identified GPCho lipids was based on correlation with the information provided from specific PI scan mode MS/MS spectra in negative ion mode (for example, PI 283 and PI 327 to monitor for lipids containing 18:0 and 22:6 fatty acyl chains, respectively), and by the use of product ion scan mode MS/MS experiments in negative ion mode at the specific *m/z* values at which individual [M+Cl]⁻ GPCho lipids were observed.

Quantitative analysis of changes in GPCho lipid abundances that occurred between control and transgenic liver mouse liver tissue was achieved by measurement of changes in the abundance of the characteristic GPCho specific *m/z* 184 product ion for a given precursor ion, compared with that of the GPCho_(14:0/14:0) internal standard, after manual correction for isotope contributions. Where more than one GPCho lipid was found to be present at a given *m/z* value, quantification was based on the combined relative abundances of the fatty acid anions that were observed in the negative ion mode MS/MS spectra. Note that characterization of the fatty acyl chains in the lipids identified here was restricted to determination of the total number of carbons and double bonds, and that information regarding their relative sites of attachment to the glycerol backbone, and the specific position of the double bonds, was not obtained. Some previous studies have suggested that the relative abundances of lipid ions observed under ESI conditions are concentration dependent, and also highly influenced by the acyl chain length and DU (24). More recently this effect has been characterized to occur under conditions of high total lipid concentration. At low concentrations, a linear correlation of ion intensity with the lipid concentration of each class is observed (25–28). In this study, although we did not know a priori the absolute concentration of the lipid extracts, mass spectra of each lipid extract were initially acquired at a range of different dilutions to determine the dilution range at which linearity in the response of specific lipids was observed. This was done in order to ensure that the ratio of specific lipid ion abundances compared with other lipids within the mixture, or compared with an internal standard, remained constant. We report here only the relative change in the abundance of the experimentally observed GPCho lipid against that of the internal standard and not the absolute concentrations of the control and transgenic mice groups to avoid ESI response difference errors.

MS/MS spectra shown were typically acquired for a period of 2.5–10 min. A five-point Gaussian smooth was applied to all spectra prior to data analysis. Student's *t*-test of dependent samples

was performed for all analyses. Data values are displayed as mean \pm SD. All solvents used were filtered HPLC grade. Methanol (MeOH) was purchased from J.T. Baker (Phillipsburg, NJ). Hydrochloric acid (HCl), ammonium hydroxide (NH₄OH), and chloroform (CHCl₃) were from EMD Chemicals (Gibbstown, NJ). Synthetic phospholipid standards were purchased from Avanti Polar Lipids Inc. (Alabaster, AL).

Western blots

Proteins were extracted from the transgenic and control liver tissues using a radio immuno precipitation assay buffer and separated using sodium dodecyl sulfate-polyacrylimide gel electrophoresis (SDS-PAGE) gels. A nitrocellulose membrane (0.45 μ m pore size) was used for transfer of the proteins. Antibodies against SCD1, FADS2, and fatty acid desaturase 1 (FADS1) were utilized for enzyme expression detection. Visualization of the proteins was achieved by 5-bromo-4-chloro-3-indolyl phosphate/nitro blue tetrazolium labeling of alkaline phosphatase secondary antibodies. The SCD1 antibody was a mouse monoclonal (Santa Cruz Biotechnology, Inc., Santa Cruz, CA), and the FADS2 antibody was a rabbit anti-mouse polyclonal antibody (Alpha Diagnostic International, San Antonio, TX). The FADS1 antibody used was a rabbit anti-human polyclonal antibody (ProteinTech Group, Inc., Chicago, IL).

Microarray

RNA was isolated from the liver tissue and further purified using an RNeasy Mini Kit (Qiagen, Valencia, CA) and the RNA cleanup protocol provided. After purification, the RNA concentration was determined with a Nanodrop scanning spectrophotometer, and then qualitatively assessed for degradation using the ratio of 28:18s rRNA obtained from a capillary gel electrophoresis system (Agilent 2100 Bionalalyzer, Agilent Technologies).

The Illumina TotalPrep™ RNA Amplification Kit was used for labeling cRNA (Ambion, Austin, TX). Briefly, 200 ng of total RNA was primed with T7-oligo-dT and reverse transcribed, followed by production of double-stranded cDNA with *E. coli* DNA polymerase. cRNA was transcribed in vitro from the T7 promoter using a biotinylated ribonucleotide analog. cRNA was hybridized to HumanRef-8 v2 Expression BeadChips as specified by Illumina (San Diego, CA). BeadChips were washed and stained according to the Illumina protocol and scanned with an Illumina BeadArray Reader.

Illumina BeadStudio software was used to quantitate the signal from BeadChips, and the MATLAB normalized values were imported into BRB ArrayTools (Biometric Research Branch, National Cancer Institute) where they were then log transformed. Genes that fell below the 50th percentile of gene variance were excluded from the results. We identified genes that were differentially expressed between any two classes by using a multivariate permutation test (29, 30). We used the multivariate permutation test to provide a median false discovery rate (FDR) of 5% (90% confidence). The test statistics used were random variance t-statistics for each gene (31). Genes that were differentially expressed (<5% FDR) and simultaneously had a ratio 2-fold or larger were used in further analyses.

Pathways were explored by placing the data of genes that only passed our significance/ratio threshold into Ingenuity Pathways Analysis (Ingenuity® Systems, www.ingenuity.com).

Statistical analysis

Statistical analysis of the data produced by the various experiments was performed, utilizing a Student's *t*-test of independent samples between control and transgenic mice at each time point.

Two-way ANOVA (GraphPad Prism 5 software, La Jolla, CA) was used to determine significant changes between control and transgenic mice over the time course assessed. A difference was assessed between the control and transgenic mice peak area values for each fatty acid in question and the ANOVA was then applied.

RESULTS

Histology and MRI results

Histological analysis of the tissue from the transgenic mice reveals small but noticeable nodules forming at 30 weeks of age in the male mouse liver tissue (Fig. 1A). There was slight steatosis and nuclear pleomorphism noticeable in the nodules of these 30-week-old mice. At 40 weeks of age in these mice, rampant nodular and tumor growth was observed in the liver sections with severe nuclear pleomorphism accompanied with steatosis and loss of liver lobule structure (Fig. 1C). MRI images of the transgenic mice showed the development of nodules in two males at 26 weeks of age and three other males at 30 weeks of age; all other animals had evidence of nodular formations at later time points (Fig. 2A). The minimal lesion size was a 2.7 \times 2.4 mm nodule at 26 weeks of age. A plot of tumor volume growth shows an exponential increase for the transgenic mice, compared with no detected tumors for control CD1 mice (Fig. 2B). A significant difference ($P < 0.03$) was found between transgenic mice at 30 weeks compared with transgenic mice at 40 weeks of age. Pathologic analysis of histology slides was able to confirm the neoplasms noted in the MRI images.

MRS results

A relationship of the 2.8 to 5.3 ppm MRS detectable lipid peaks to the number of double bonds in fatty acyl groups is illustrated in Fig. 3. The curve was generated

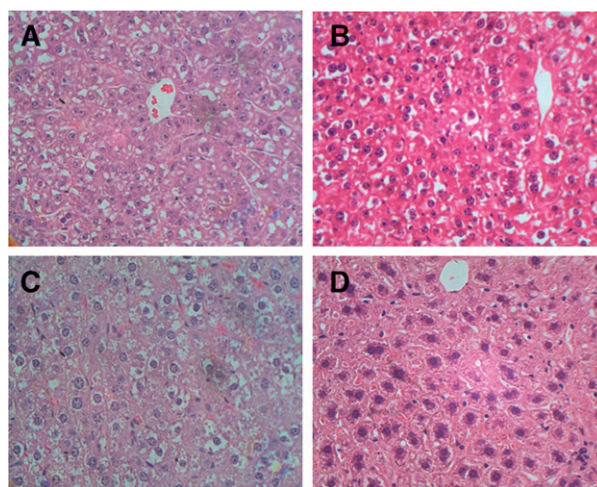


Fig. 1. Histological sections of liver tissue from TGf α / *c-myc* mice at (A) 30, (B) 34, and (C) 40 weeks of age respectively highlighting the nodular regions in the tissue. Note the occurrence of nuclear pleomorphism and steatosis as early as 30 weeks (A). CD1 control liver tissue section at 40 weeks of age (D).

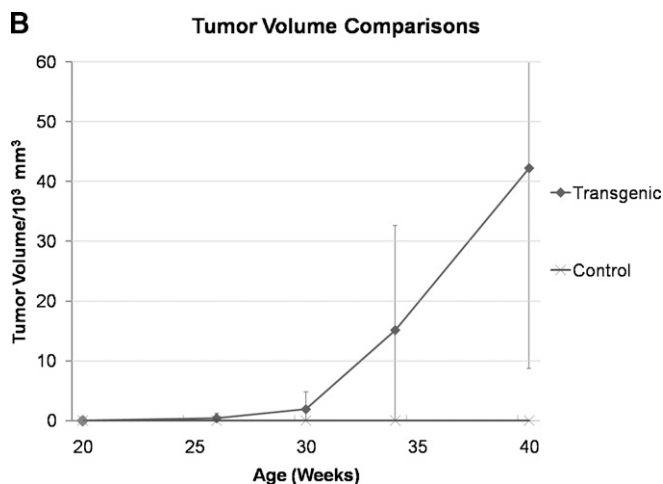
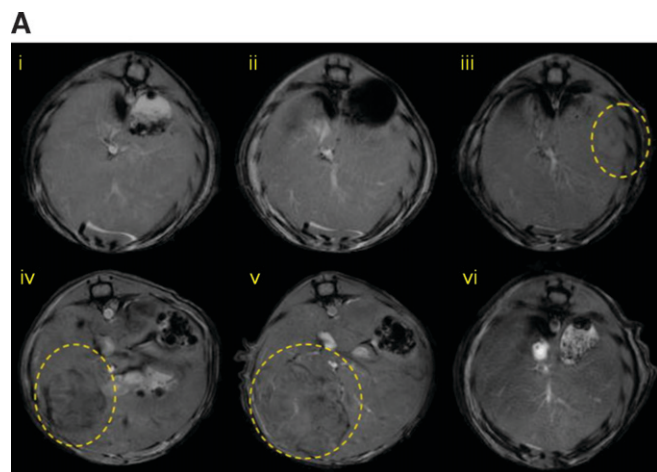


Fig. 2. A: Representative MR images (single slices from multiple slice data sets) of the liver regions of TGF α /c-myc mice at 20 (i), 26 (ii), 30 (iii), 34 (iv), and 40 (v) weeks, depicting the development of nodules (iii) and tumors (iv and v). A comparative representative image of a control CD1 mouse liver at 40 weeks is also displayed (vi). Outlined regions depict nodules and/or tumors. B: Liver tumor volumes measured from multiple MRI image slices taken through the livers of TGF α /c-myc mice and CD1 mice from 20 to 40 weeks of age (N = 5 animals per time point). The large variability is attributed to the data sets being a combination of male and female tumor volumes. The females developed neoplasia much later than the males. Error bars represent mean \pm SD.

using pure fatty acid standards. In Fig. 3, a decrease in the R value corresponds to a decrease in the number of double bonds in the fatty acids. This relationship can be explained by the formula:

$$n_{\text{bonds}} = -1/(R-1)$$

In this formula, the number of bonds is equal to the reciprocal value of R (2.8 ppm peak divided by the 5.3 ppm peak) minus 1, because R can never be more than 1 (12). The average R value for the transgenic mice at each experimental time point is plotted on the graph (depicted by the diamond shape). The R values of the transgenic mice indicate that as the mice age, the fatty acids in the liver are predominantly monounsaturated ($n_{\text{bonds}} = 1$). Fig. 4A depicts a representative spectrum from the MRS

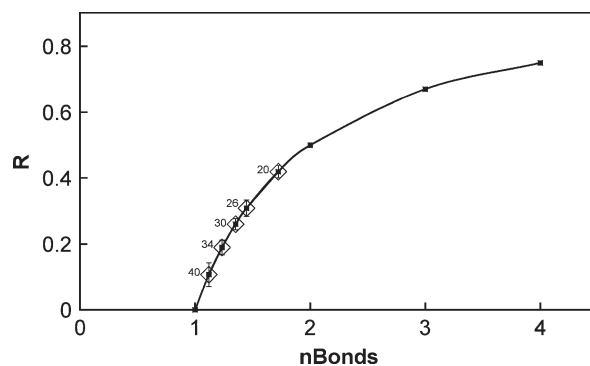


Fig. 3. The relationship of the 2.8 ppm to 5.3 ppm ratio (R) of lipid peaks, detected by magnetic resonance spectroscopy (MRS) to the number of double bonds (nBonds). Note that as the R decreases so does nBonds. The integral ratio values of the TGF α /c-myc mice from the study are also plotted on the line with the data points identified by their age in weeks (from 20 to 40 weeks). The integral ratio values of the TGF α /c-myc mice indicate that as they get older, the fatty acids tend to be predominately monounsaturated (nBonds = 1), such as in oleic acid.

data that was obtained from a selected ROI that corresponded to tumor development in TGF α /c-myc mice. From MRS analysis a significant decrease in the DU, 2.8 ppm peak ($-\text{CH} = \text{CH}-\text{CH}_2-\text{CH} = \text{CH}-$)/5.3 ppm peak ($-\text{CH} = \text{CH}-$), of the fatty acyl groups in the lipids was revealed over time (Fig. 4B). Fig. 4B was generated utilizing averages of DU values for each of the animals at a particular time point. Measurements were obtained from the spectra if the peak of interest was at least five times the baseline noise. The CD1 control and TGF α /c-myc transgenic mice began with a DU close to 0.45 at 20 weeks, which represents a high level of linoleic acid (Fig. 3). By 26 weeks, there was a significant ($P < 0.001$) difference between the DU of the control mice and the DU in the transgenic mice. At subsequent time points, the DU in the transgenic mice decreased to an end point of 0.1, which represents a high level of oleic acid (Fig. 3). Meanwhile, the control mice remained relatively constant in their DU, maintaining an average value of 0.4. By the 40-week time point, there was a noticeable difference in the spectra of transgenic versus control mice, with the bis-allyl 2.8 ppm peak (representative of fatty acids with more than one double bond) becoming generally much smaller in the transgenic mice compared with controls (Fig. 5). Two-way ANOVA analysis of the transgenic and control mouse DU values revealed a significant difference ($P < 0.05$). To eliminate any bias in voxel selection, we averaged DU values in a 4^2 voxel region in a neoplastic region and nonneoplastic region of transgenic and control mice. Fig. 6 illustrates our voxel averaging findings in a 30-week-old transgenic mouse. The sixteen voxel average DU values of the neoplastic region were 0.298, while the average DU value for the nonneoplastic region was 0.424.

HPLC and mass spectrometry results

HPLC analysis of the liver tissues removed from the transgenic and control mice at each of the MRS time points revealed alterations in the amounts of several fatty

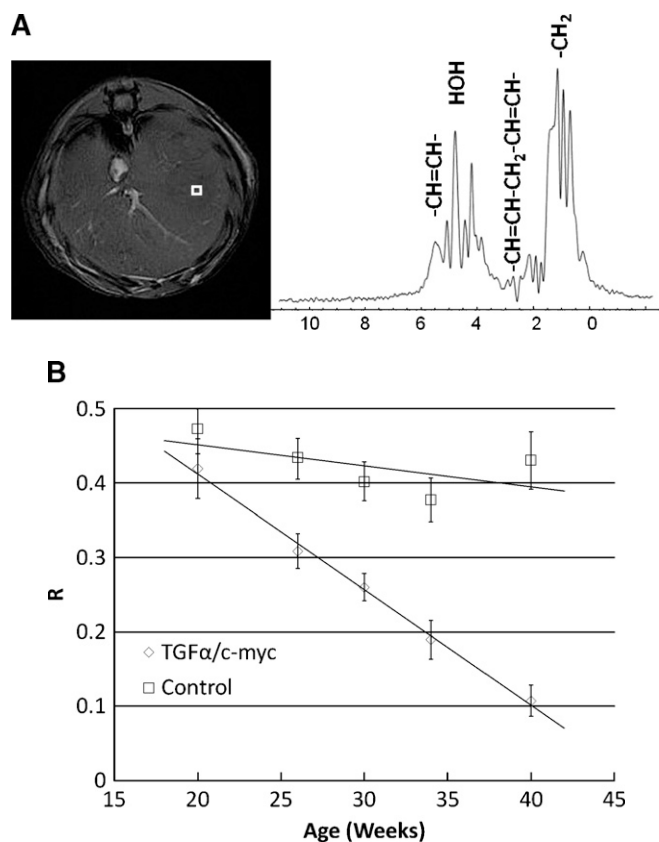


Fig. 4. A: MR image (left) of a TGFA/c-myc mouse at 40 weeks with tumors highlighting the region of interest (ROI) that the spectrum (right) was obtained from. This ROI represents a single voxel in the 32×32 matrix of voxels. Each ROI contains a unique spectrum. Spectra for the determination of the R were taken from voxels located centrally in a nodule or tumor region. The vinyl and bis-allyl proton peaks are highlighted on the spectrum. B: Average R values of TGFA/c-myc and control mice at each time point compiled from spectra such as in panel A ($n = 5$ animals per time point). Note that as the TGFA/c-myc mice age, the R decreases. This contrasts with the CD1 mice, which have a relatively constant R throughout the study. Of importance is that at 26 weeks, when there are relatively no MRI observed nodules, there is a significant difference in the R between the TGFA/c-myc mice and the CD1 control mice. This illustrates that MRS is more sensitive than MRI and could detect alterations in the R of the fatty acids that are indicative of hepatocellular carcinoma (HCC) associated neoplastic lesions. Error bars represent mean \pm SD.

acids in the PC fraction (Fig. 7A). Plots are shown as averages \pm SE. From 20 to 40 weeks in the transgenic mice, there is an increasing trend of the MUFA oleic acid as was observed in the CD1 controls (Fig. 7Ai). However, over time, the amount of oleic acid in the transgenic mice remains above that of the control mice. Two-way ANOVA comparison of the oleic acid levels in the control and transgenic mouse liver tissue revealed a significant difference ($P < 0.005$). Alterations in the PUFAs linoleic, γ -linolenic, and arachidonic acids occurred (Fig. 7Aii, iii, iv). These PUFAs had a decreasing trend in the transgenic mice over time from 20 to 40 weeks of age, while the control mice showed a gradual increase over time. A significant decrease from 20 to 40 weeks was noted in linoleic ($P < 0.005$),

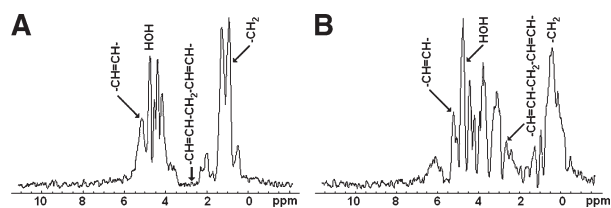


Fig. 5. Representative spectra from transgenic (A) and control (B) mice at 40 weeks of age. The vinyl (5.3 ppm), bis-allyl (2.8 ppm), water (4.7 ppm), and methyl (0.5–1.0 ppm) peaks are indicated on the spectra. Note the difference in the bis-allyl peak at 2.8 ppm between the two mice.

γ -linolenic ($P < 0.05$) and arachidonic ($P < 0.05$) acids. If a ratio of the PUFA to MUFA from the glycerol PC fraction is taken from the HPLC data, a decreasing correlation similar to the MRS ratio of the 2.8:5.3 ppm peaks appears (Fig. 4B) for the transgenic mice (Fig. 7B). Average PUFA/MUFA values of the MUFA oleic acid and combined PUFAs linoleic, γ -linolenic, and arachidonic acids from each animal were used to form the graph in Fig. 7B. HPLC analysis of individual unsaturated fatty acid peak areas indicated an absence of any notable alterations at any time point in fatty acids from the PE fraction of the transgenic and control mouse livers.

Electrospray ionization (ESI), coupled with the use of tandem mass spectrometry (MS/MS) experiments in a triple quadrupole (QqQ) mass spectrometer, revealed significant changes in the abundances of the GPCho-16:0/18:1 lipid species between the crude liver tissue extracts of 30 week control ($n = 4$) and transgenic ($n = 3$) animals (Fig. 8). The complementary information provided from a GPCho lipid class specific PI scan MS/MS experiment, to monitor the formation of a characteristic phosphocholine

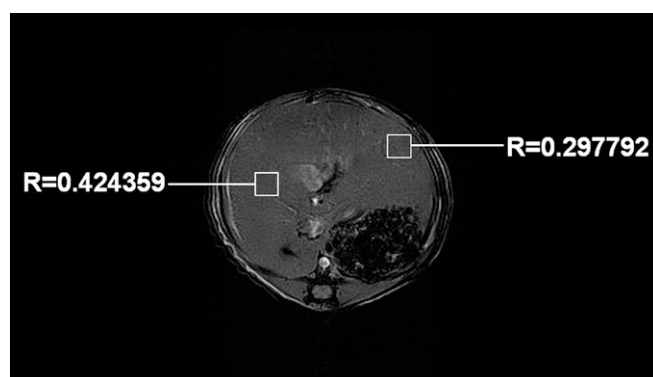


Fig. 6. MR image of a 30-week-old mouse with an apparent neoplasm with 4^2 average degree of unsaturation (DU) (or R) values, obtained using chemical shift imaging (CSI), of the nodular and nonnodular regions displayed. The DU of the nodular region is much lower than the nonnodular region and is similar to the average DU value of transgenic mice found for the 30-week time point as shown in Figure 4B. The nonneoplastic DU value is similar to what was observed for the average control mice DU value at 30 weeks in Figure 4B.

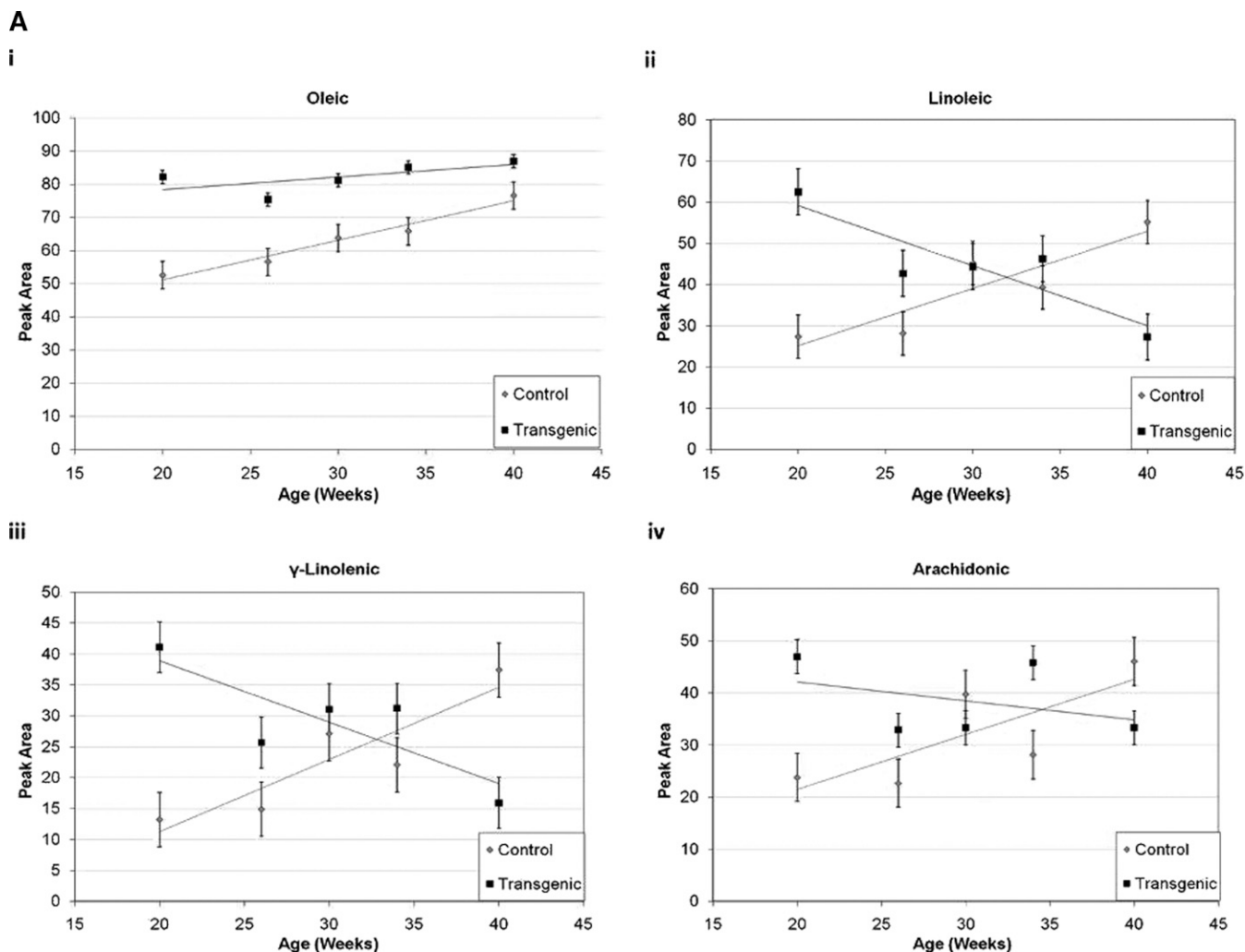


Fig. 7. A: HPLC analysis of fatty acyl species from the glycerol phosphatidylcholine (GPCho) fraction of phospholipids found in the transgenic (■) and control (◆) mouse liver tissue revealed several altering trends in oleic (i), linoleic (ii), γ -linolenic (iii), and arachidonic (iv) fatty acids. Results are shown as averages of $n \geq 3$ animals/time point for the transgenic mice and $n = 3$ animals/time point for the control mice \pm SE. There was a gradual increase in oleic acid (A) over time based off of HPLC analysis ($R^2 = 0.4069$). There was a greater amount of oleic acid in the transgenic mice (■) at all time points over the control mice (◆). A decreasing trend for linoleic acid (B) was observed in the transgenic mice (■) from 20 to 40 weeks of age upon HPLC analysis of the liver tissue ($R^2 = 0.7851$). This trend is directly opposite of what is seen in the control mouse liver tissue (◆). There was an overall decrease in γ -linolenic acid (C) from 20 to 40 weeks of age in the transgenic mice (■) as opposed to control mice (◆) based off HPLC analysis ($R^2 = 0.6731$). Arachidonic acid (D) amounts for the transgenic mice (■) decreased from 20 to 40 weeks of age in the transgenic mice ($R^2 = 0.1473$), while there was a gradual increase in arachidonic acid observed in the control mice (◆). B: The ratio of PUFA to MUFA based off of the HPLC data sets shows a decreasing trend similar to the MRS ratio of the 2.8:5.3 ppm peaks (Figure 4B) appears for the transgenic mice (■). This indicates that the level of PUFAs is decreasing over time while the MUFA levels are increasing. The control mouse (◆) trend indicates a greater increase in PUFAs over MUFA from 20 to 40 weeks of age. Results are shown \pm SE.

product ion at m/z 184 (PI 184) in positive ion mode, as well as fatty acyl group specific PI MS/MS scans or product ion MS/MS scan experiments in negative ion mode, were employed to elucidate the identity of the head group, as well as the identities of the fatty acyl chains (number of total carbons and double bonds), within the lipid of interest. For these samples, an internal standard consisting of a GPCho_(14:0/14:0) lipid was added prior to mass spectrometry analysis. Quantification was achieved by measurement of changes in the abundance of the experimentally observed GPCho lipid abundance against that of the internal standard, for the control and transgenic mice groups. A

>2-fold change ($P > 0.05$) was observed in the abundance of the GPCho_(16:0/18:1) lipid (m/z 760.3), while a >1.5-fold change [$P > 0.05$ (i.e., not significant)] was observed in the abundance of GPCho_(16:0/22:6) (m/z 806.3). Although assessed there were no significant differences in GPE lipids (data not reported).

Western blot results

Western blot analysis of the male transgenic and male control mouse liver tissue was performed. A Student's *t*-test of independent values revealed there was a significant increase in SCD1 ($P < 0.05$) at the 34-week time point in the

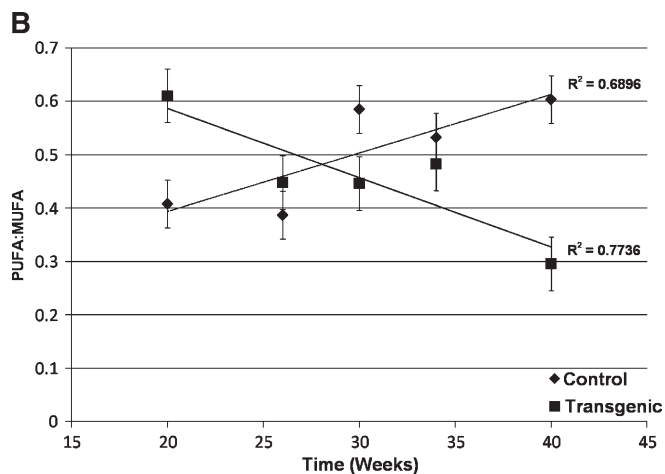


Fig. 7.—Continued.

transgenic mice compared with the control mice (Fig. 9). Representative images of the blots from the 40-week time point are included in Fig. 9. FADS2 enzyme levels, responsible for γ -linolenic acid formation, remained stationary over time in the transgenic mice, while the control mice FADS2 levels were shown to gradually increase from 20 to 40 weeks of age, although there was no significant difference between transgenic and control mice at any time-point or over the time-course studied (data not shown). Although an increasing trend of FADS2 levels in transgenic mice at 20 weeks of age is present, the increase was found to be not significant ($P > 0.05$). FADS1 ($\Delta 5$ desaturase), responsible for the formation of arachidonic acid, showed no significant alteration in enzyme levels over time in the transgenic versus control mice (data not shown).

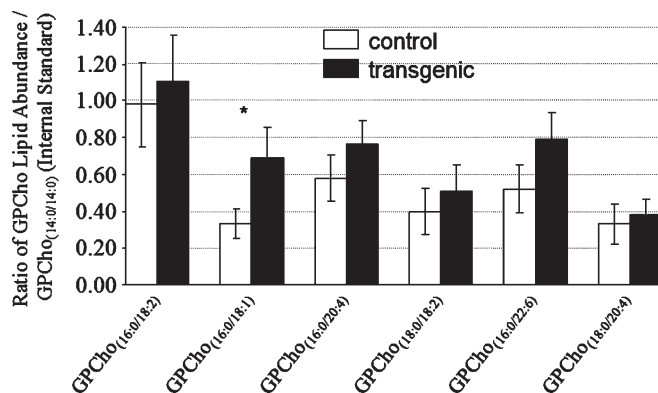


Fig. 8. Quantitative ESI-MS/MS analysis of glycerol phosphatidylethanolamine (GPE) lipids in the crude liver tissue extracts of 30-week control ($n = 4$) and TGF α / *c-myc* ($n = 3$) mice. A >2 -fold change ($* P > 0.025$, one-tailed *t*-test with pooled estimation of variance) was observed in the abundance of GPCho_(16:0/18:1) (m/z 760.3), (measured as the change in ratio of GPCho_(14:0/14:0) / GPCho_(16:0/18:1) between the control and TGF α / *c-myc* mice groups), while a >1.5 -fold change ($P > 0.05$, one-tailed *t*-test with pooled estimation of variance) was observed in the abundance of GPCho_(16:0/22:6) (m/z 806.3).

Microarray results

Microarray analysis of male transgenic and male control tissue at 30 weeks, with a 3-fold change and 5% false discovery rate (FDR), presented us with several interesting findings regarding lipid metabolism. Three of the top six canonical pathways affected in the transgenic versus control data set were related to lipid metabolism. For the purposes of this study we focused solely on the lipid metabolism pathways. The top canonical pathway affected in the transgenic mice when compared with controls is that of linoleic acid metabolism ($P = 7.89E-07$). Some of the up-regulated genes associated with this pathway are several members of the cytochrome P450 (CYP) family, involved in fatty acid and xenobiotics metabolism in the liver, including CYP2B9, CYP2B13, and CYP2C18 (Fig. 10A). There were many down-regulated genes associated with linoleic acid metabolism including: CYP2C37, CYP2C50, CP2C54, CYP2D13, CP4A22, CP4F8, and PNPLA3. Arachidonic acid metabolism was another highly affected canonical pathway (fourth overall) when comparing the transgenic and control mice ($P = 1.33E-04$). The same genes affected in linoleic acid metabolism were also involved in the alterations in arachidonic acid metabolism. The desaturase enzyme SCD2 was found to be up-regulated (3-fold) in the transgenic tissue as compared with the control tissue with an exponential value of 12.200 (Fig. 10B). This enzyme is involved in the formation of oleic acid from stearoyl-CoA.

DISCUSSION

The findings of this study have shown that MRS is able to detect *in vivo* alterations in phospholipid unsaturated fatty acyl hydrogens in a transgenic mouse model of HCC that correlates with neoplastic lesion formation. Significant alterations in the levels of unsaturated of fatty acyl lipids were noted as early as 26 weeks of age in the transgenic mice, a time point where MRI, the standard diagnostic imaging technique, was only able to detect neoplasms in a few cases. Coinciding with the MRS results, we have corroborating experimental evidence utilizing other methods (HPLC, ESI-MS/MS, Western blot, and microarray) that showed there were hepatocarcinogenesis-associated alterations in the unsaturated fatty acids, desaturase enzyme levels, and gene expression. MRS was able to detect a significant difference ($P < 0.001$) in the DU of the fatty acids of lipids in the liver at a time point (26 weeks) before there were any significant detectable lesions (e.g., nodules or tumors) by MRI in almost all of the transgenic animals, compared with CD1 control mice. The MRS CSI method was used to establish where in the liver the DU ratio was lowest. In most of the transgenic mice ($>95\%$), these regions of low DU coincided with MRI detection of visual nodules or tumors that appeared at later time points. The spectra used to determine the DU value were taken from the same anatomical ROI at each time point. The anatomical ROI was determined by using MRI images of the TGF α /*c-myc* mouse livers at stages where visually ap-

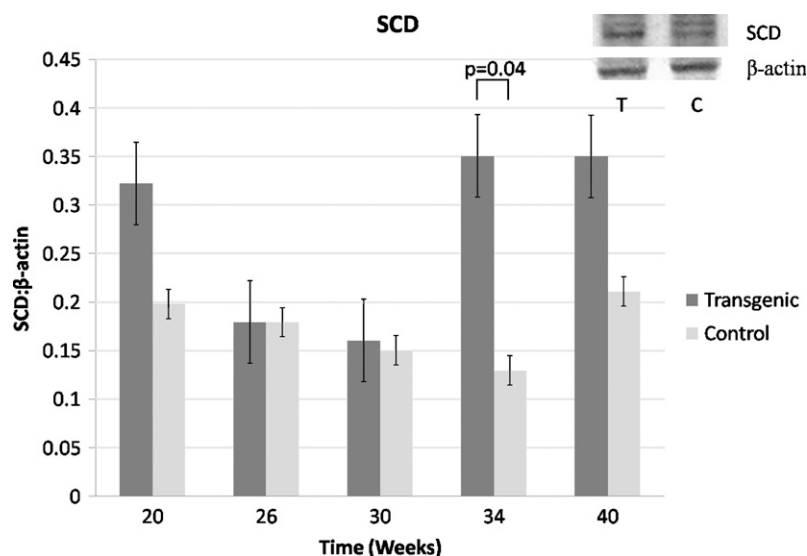


Fig. 9. Western blot analysis for stearoyl CoA desaturase (SCD) enzyme levels reveals that a ratio of the optical density of SCD bands to β -actin loading control bands shows a gradual increase in SCD levels over time in the transgenic mice (dark bars) while the SCD levels in the control mice (light bars) remain relatively constant over time. Representative images of the Western blots from the 40 week time point are shown for the transgenic (T) and control (C) mouse liver tissue. Results are shown as an average of $n \geq 3$ animals/time point \pm SE.

parent nodular or tumor growth was observed. We then backtracked through earlier time points, selecting the same ROI in the animals at each time until we selected a time and corresponding ROI with no visual neoplastic lesions in the MRI images. By moving forward in time, we could conceivably use the decreased DU ratios to predict where a neoplastic formation would occur.

The HPLC results support our MRS data, where in the transgenic mice there is an increase in the level of the MUFA oleic acid and decreases in the levels of the PUFAs linoleic, γ -linolenic, and arachidonic acids over time during neoplastic growth development. The ESI-MS/MS results from lipids extracts obtained at 30 weeks revealed an increase in the abundance of certain GPCho lipids containing palmitic and oleic acids. We chose to utilize the 30-week time point for ESI-MS/MS analysis of the liver tissue to try and clarify what changes are occurring at this juncture, because we observed an increase in neoplastic formations by MRI and histology in many of the transgenic mice at this time. Conversely, the HPLC results showed no significant alterations in unsaturated lipids between the transgenic and the control groups at 30 weeks. We postulate that the lack of detectable changes in the unsaturated fatty acyl PCs in the transgenic and control mice at the 30 week time point is due to decreasing levels occurring in the transgenic mice while there is an increasing level in the CD1 controls resulting in a cross-over being reached in the fatty acid levels between both groups at this time-point (Fig. 7A).

With the MRS data, we are measuring the peak areas of the bis-allyl or allylic methylene hydrogen protons at 2.8 ppm ($-\text{CH}_2-\text{CH}_2-\text{CH}=\text{}$; found only in PUFAs) and the vinyl or olefinic methylene hydrogen protons at 5.3 ppm ($-\text{CH}=\text{CH}-$; found in all unsaturated fatty acids, but the only peak that would be seen in MUFA) of mobile lipids. A related recent study in humans was conducted using a MR spectroscopic imaging method to determine the levels of PUFAs in cancerous breast tissues, where they found that decreased PUFA levels were present in an invasive ductal

carcinoma of a breast cancer patient compared with healthy breast tissue (32). In that study selective multiple-quantum coherence transfer was used to detect the same lipid hydrogens that we used to calculate a DU ratio in our mouse study, which were the bis-allyl hydrogen protons of the unsaturated acyl chain at 2.8 ppm coupled to the vinyl hydrogen protons of PUFA at 5.3 ppm (32).

In our study, when we compared the PUFA values taken from the HPLC data to the MUFA values, we observed a correlation similar to the MRS ratio of the bis-allyl to vinyl protons. The measurements in the MRS data are from ratio comparisons of hydrogen atoms (the methylene hydrogens between the double bonds, compared with the vinyl hydrogens on the double bonds) on unsaturated fatty acyl groups of mobile lipids, and not direct measurements of the relative amount of hydrogen atoms in individual unsaturated fatty acyl lipid groups. As such, while we are measuring all fatty acyl groups of mobile lipids in the sampling window, we are taking a ratio value that reflects alterations in MUFA and PUFA levels associated with nodule and tumor formation. Changes in individual molecular species, as was obtained in the HPLC and ESI-MS/MS data sets, reflect differences that may not directly correspond to the MRS data. However, the HPLC and ESI-MS/MS results can be used to correlate with the *in vivo* MRS analysis for overall fatty acyl lipid composition. We observed a significant change in unsaturated fatty acyl lipid ratios in the MRS data during hepatocarcinogenesis, which directly correlated to comparative alterations in HPLC and ESI-MS/MS data.

Tying in with the HPLC measurement of fatty acid levels, the Western blot data for some desaturase enzymes, particularly SCD1, involved in the synthesis of unsaturated fatty acids also had corresponding changes. From the Western blot data on FADS2 enzyme levels we noticed some alteration from 20 to 40 weeks of age in the transgenic mice when compared with controls; however, it was not significant. It is believed that impairment in FADS2 function would result in an increase in FA substrates, such as oleic

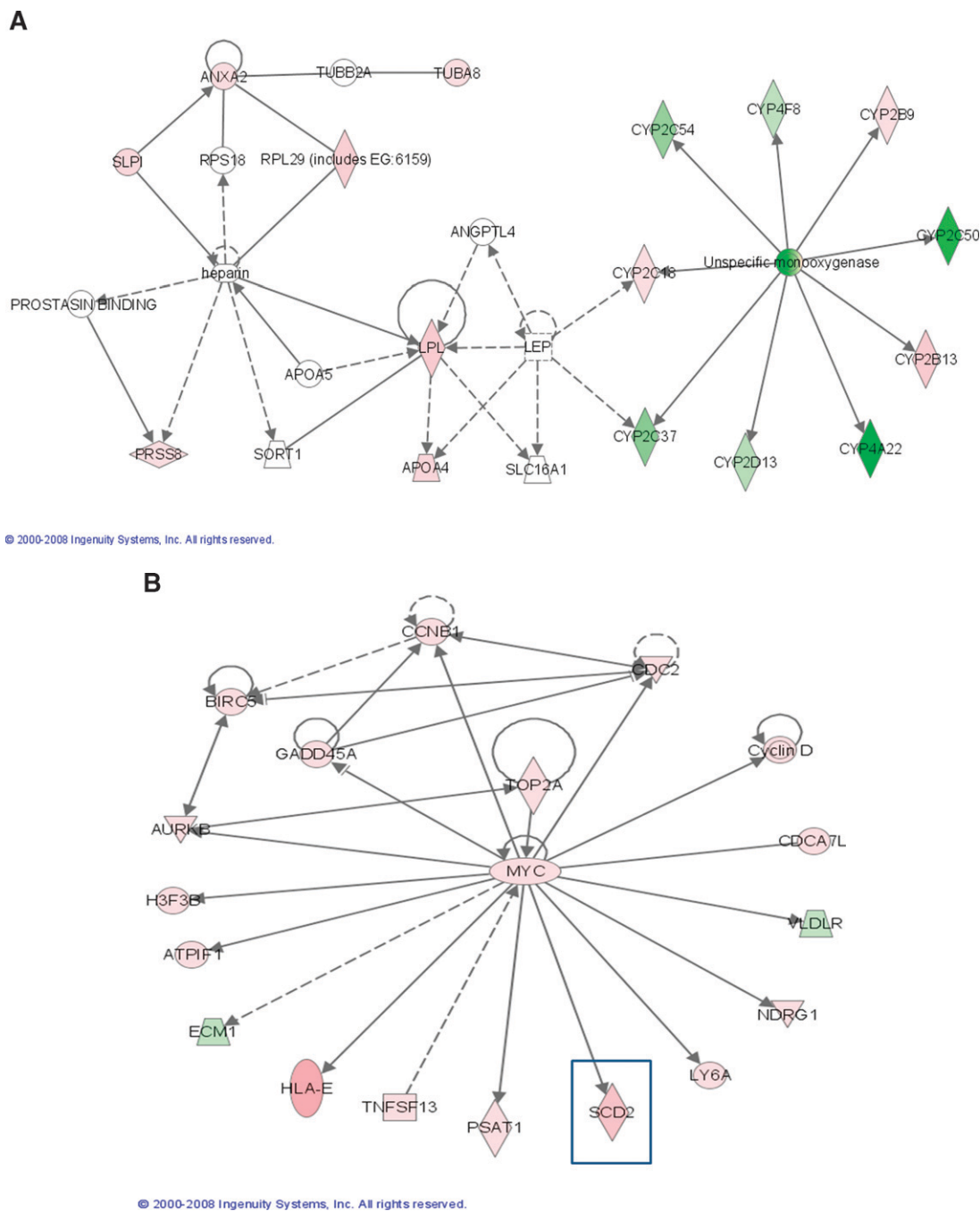


Fig. 10. A: Pathway analysis of isolated RNA from transgenic ($n = 3$), compared with control liver ($n = 3$) tissue, at 40 weeks revealed up-regulation (depicted by a red color) and down-regulation (depicted by a green color) in several genes involved in lipid metabolism with a 3-fold difference and 5% false discovery rate (FDR). B: Pathway analysis of isolated RNA from transgenic ($n = 3$), compared with control liver ($n = 3$) tissue, at 40 weeks of age. The *c-myc* gene is mutated in the transgenic mice and leads to an up-regulation of several genes. The most notable increase in relation to unsaturated lipid metabolism is SCD2 with a 3-fold increase in transgenic mice compared with controls and 5% FDR.


acid (4). Indeed, the findings of our study show an increase in oleic acid levels. The increased SCD level observed in the Western blots (Fig. 9) in the transgenic tissue, when compared with the control tissue, supports the findings that there is an increase in oleic acid in the transgenic mice, particularly at week 34. The results of the Western data for SCD1 at week 34 support our HPLC and MRS results, which indicate an increase of MUFA (as

observed from MRS data), such as oleic acid (as observed from HPLC and ESI-MS/MS data).

Interestingly, in our microarray analysis of the tissue, there were many genes seen to be either up-regulated or down-regulated in the transgenic mice when compared with the controls. One noted change related to fatty acid metabolism was in SCD2, a desaturase enzyme involved in oleic acid formation, which is more highly expressed in

embryonic liver. The significance of this finding is that SCD2 expression in the adult normal liver is much lower at 40 weeks in comparison to embryonic liver. It would appear that SCD2 may be partly responsible for the increase in MUFA oleic acid in the transgenic liver tissue, as detected by microarray analysis, along with SCD1, as detected by Western blots. Pathway analysis of the microarray data reveals that SCD2 is directly acted upon and upregulated by *c-myc*. The mutation and subsequent increase in *c-myc* expression in our mice would lend to the increase in SCD2 up-regulation.

We utilized the CSI method to obtain our spectra in order to overcome one of the common arguments against MRS as a diagnostic tool, the fact that traditional MRS obtains only a single spectrum from one region of the liver. With CSI, we are able to obtain a series of unique spectra from different spatial regions in a 1.5 mm thick slice of the liver in order to look for any alterations in the fatty acid profile in heterogeneous tissue. One drawback to CSI is the effect known as chemical shift drift, which occurs when the peaks in spectra adjacent to one another have a gradual shift in the position of the metabolites, resulting in some metabolites not being in the correct position on the ppm scale. In order to overcome this drawback, the center most spectrum in the CSI matrix was determined and a correction formula was applied to all spectra that adjusted the ppm scale accordingly. The main focus of this study was to show the ability of MRS to detect in vivo alterations in the DU of fatty acyl groups from lipids in the livers of transgenic mice that developed neoplasia. Additional MRS analysis could identify specific species of fatty acyl groups of lipids in vivo, but that would involve using 2-dimensional (^1H and ^{13}C) MRS methods requiring different RF coils other than were utilized in this study and potentially longer acquisition times.

Overall, we have shown that MRS can be used to detect alterations in lipid metabolism associated with hepatocarcinogenesis in the mouse liver in vivo before nodules or tumors are visually seen with MRI in most cases. There was a significant difference in the DU between the transgenic mice and control mice at 26 weeks of age while there were MRI visible lesions noted at this time point in only two animals out of 20. HPLC, Western blot, and microarray data all support our MRS findings with correlative alterations in the expression of MUFA and PUFA noted by all of the corroborating experiments. The usefulness of MRS in providing early detection metabolic information associated with primary liver cancer in mice is evident and the application of similar methods to clinical studies should be further pursued. 

TGF α / *c-myc* mice were kindly obtained from Dr. S.S. Thorgeirsson at the National Cancer Institute (NCI), Bethesda, Maryland. The authors would like to thank the Oklahoma Medical Research Foundation microarray core-facility for their invaluable assistance. We would also like to thank Dr. Charles Stewart for his help in preparing the liver tissue for microarray analysis, Ms. Jenny Oblander for her assistance in preparing and staining the tissue for histologic analysis, Dr. Dee Wu and

Mr. Rajibul Alam for their assistance in tumor volume measurements, and Mr. Todd Lydic for his assistance with the mass spectrometry analysis.

REFERENCES

1. World Cancer Report, S. B. W. a.P. Kleihues, Editor. 2003, World Health Organization: Lyon. p. 203–207.
2. Qin, Y., M. Van Cauteren, M. Osteaux, and G. Willems. 1992. Quantitative study of the growth of experimental hepatic tumors in rats by using magnetic resonance imaging. *Int. J. Cancer*. **51**: 665–670.
3. Towner, R. A., H. Hashimoto, and P. M. Summers. 2000. Non-invasive in vivo magnetic resonance imaging assessment of acute aflatoxin B1 hepatotoxicity in rats. *Biochim. Biophys. Acta*. **1475**: 314–320.
4. Abel, S., C. M. Smuts, C. de Villiers, and W. C. A. Gelderblom. 2001. Changes in essential fatty acid patterns associated with normal liver regeneration and the progression of hepatocyte nodules in rat hepatocarcinogenesis. *Carcinogenesis*. **22**: 795–804.
5. Ntambi, J. M., and H. Bene. 2001. Polyunsaturated fatty acid regulation of gene expression. *J. Mol. Neurosci*. **16**: 273–278.
6. Begin, M. E., U. N. Das, G. Ells, and D. F. Horrobin. 1985. Selective killing of human cancer cells by polyunsaturated fatty acids. *Prostaglandins Leukot. Med*. **19**: 177–186.
7. Gelderblom, W. C. A., W. Moritz, S. Swanevelde, C. M. Smuts, and S. Abel. 2002. Lipids and $\Delta 6$ -desaturase activity alterations in rat liver microsomal membranes induced by fumonisin B₁. *Lipids*. **37**: 869–877.
8. Jiang, W. G., R. P. Bryce, D. F. Horrobin, and R. E. Mansel. 1998. Regulation of tight junction permeability and occludin expression by polyunsaturated fatty acids. *Biochem. Biophys. Res. Commun.* **244**: 414–420.
9. Bolan, P. J., S. Meisamy, E. H. Baker, J. Lin, T. Emory, M. Nelson, L. I. Everson, D. Yee, and M. Garwood. 2003. In vivo quantification of cholin compounds in the breast with ^1H MR spectroscopy. *Magn. Reson. Med*. **50**: 1134–1143.
10. He, Q., R. Z. Xu, P. Shkarin, G. Pizzorno, C. H. Lee-French, D. L. Rothman, D. C. Shungu, and H. Shim. 2003–2004. Magnetic resonance spectroscopic imaging of tumor metabolic markers for cancer diagnosis, metabolic phenotyping, and characterization of tumor microenvironment. *Dis. Markers*. **19**: 69–94.
11. Singer, S., M. Sivaraja, K. Souza, K. Millis, and J. M. Corson. 1996. ^1H -NMR detectable fatty acyl chain unsaturation in excised leiomyosarcoma correlate with grade and mitotic activity. *J. Clin. Invest.* **98**: 244–250.
12. Tesiram, Y. A., D. Saunders, and R. A. Towner. 2005. Application of proton NMR spectroscopy in the study of lipid metabolites in a rat hepatocarcinogenesis model. *Biochim. Biophys. Acta*. **1737**: 61–68.
13. Foley, L. M., R. A. Towner, and D. M. Painter. 2001. In vivo image-guided ^1H -magnetic resonance spectroscopy of the serial development of hepatocarcinogenesis in an experimental animal model. *Biochim. Biophys. Acta*. **1526**: 230–236.
14. Tesiram, Y. A., D. Saunders, and R. A. Towner. 2008. Chemical speciation by selective heteronuclear single-quantum coherence spectroscopy: determination of double-bond quantity in unsaturated fatty acid compounds. *NMR Biomed*. **21**: 345–356.
15. Kurhanewicz, J., M. G. Swanson, S. J. Nelson, and D. B. Vigneron. 2002. Combined magnetic resonance imaging and spectroscopic imaging approach to molecular imaging of prostate cancer. *J. Magn. Reson. Imaging*. **16**: 451–463.
16. Nelson, S. J., E. Graves, A. Pirzkall, X. Li, A. Antiniw Chan, D. B. Vigneron, and T. R. McKnight. 2002. In vivo molecular imaging for planning radiation therapy of gliomas: an application of ^1H MRSI. *J. Magn. Reson. Imaging*. **16**: 464–476.
17. Kaji, Y., A. Wada, I. Imaoka, M. Matsuo, T. Terachi, Y. Kobashi, K. Sugimura, M. Fujii, K. Maruyama, and O. Takizawa. 2002. Proton two-dimensional chemical shift imaging for evaluation of prostate cancer: external surface coil vs. endorectal surface coil. *J. Magn. Reson. Imaging*. **16**: 697–706.
18. Liimatainen, T. 2006. J.H., I. Tkac, O. Grohn, Ultra-short echo time spectroscopic imaging in rats: implications for monitoring lipids in glioma gene therapy. *NMR Biomed*. **19**: 554–559.
19. Fayad, L. M., D. A. Bluemke, E. F. McCarthy, K. L. Weber, P. B. Barker, and M. A. Jacobs. 2006. Musculoskeletal tumors: use of

- proton MR spectroscopic imaging for characterization. *J. Magn. Reson. Imaging*. **23**: 23–28.
20. Murakami, H., N. D. Sanderson, P. Nagy, P. A. Marino, G. Merlino, and S. S. Thorgeirsson. 1993. Transgenic mouse model for synergistic effects of nuclear oncogenes and growth factors in tumorigenesis: interaction of c-myc and transforming growth factor α in hepatic oncogenesis. *Cancer Res.* **53**: 1719–1723.
21. Calvisi, D. F., and S. S. Thorgeirsson. 2005. Molecular mechanisms of hepatocarcinogenesis in transgenic mouse models of liver cancer. *Toxicol. Pathol.* **33**: 181–184.
22. Folch, J., M. Lees, and G. H. Sloane-Stanley. 1957. A simple method for the isolation and purification of total lipids from animal tissues. *J. Biol. Chem.* **226**: 497–509.
23. DeMar, J. C., and R. E. Anderson. 1997. Identification and quantitation of the fatty acids composing the vCoA ester pool of bovine retina, heart, and liver. *J. Biol. Chem.* **272**: 31362–31368.
24. Koivusalo, M., P. Haimi, L. Heikinheimo, R. Kostianen, and P. Somerharju. 2001. Quantitative determination of phospholipid compositions by ESI-MS: effects of acyl chain length, unsaturation, and lipid concentration on instrument response. *J. Lipid Res.* **42**: 663–672.
25. Han, X., and R. W. Gross. 2005. Shotgun lipidomics: electrospray ionization mass spectrometric analysis and quantitation of cellular lipidomes directly from crude extracts of biological samples. *Mass Spectrom. Rev.* **24**: 367–412.
26. Han, X., K. Yang, J. Yang, K. N. Fikes, H. Cheng, and R. W. Gross. 2006. Factors influencing the electrospray intrasource separation and selective ionization of glycerophospholipids. *J. Am. Soc. Mass Spectrom.* **17**: 264–274.
27. Mitchell, T. W., K. Ekroos, S. J. Blanksby, A. J. Hulbert, and P. L. Else. 2007. Differences in membrane acyl phospholipid composition between an endothermic mammal and an ectothermic reptile are not limited to any phospholipid class. *J. Exp. Biol.* **210**: 3440–3450.
28. Deeley, J. M., T. W. Mitchell, X. Wei, J. Korth, J. R. Nealon, S. J. Blanksby, and R. J. W. Truscott. 2008. Human lens lipids differ markedly from those of commonly used experimental animals. *Biochim. Biophys. Acta.* **1781**: 288–298.
29. Simon, R., E. Korn, L. McShane, M. Radmacher, G. Wright, and Y. Zhao. 2003. Design and Analysis of DNA Microarray Investigations. Springer-Verlag, New York.
30. Korn, E. L., J. F. Troendle, L. M. McShane, and R. Simon. Controlling the number of false discoveries: Application to high-dimensional genomic data. *J. Statist. Plann. Inference*. In press.
31. Wright, G. W., and R. Simon. 2003. A random variance model for detection of differential gene expression in small microarray experiments. *Bioinformatics.* **19**: 2448–2455.
32. He, Q., P. Shkarin, R. J. Hooley, D. R. Lannin, J. C. Weinreb, and V. I. J. Bossuyt. 2007. In vivo MR spectroscopic imaging of polyunsaturated fatty acids (PUFA) in healthy and cancerous breast tissues by selective multiple-quantum coherence transfer (Sel-MQC): A preliminary study. *Magn. Reson. Med.* **58**: 1079–1085.